Journal of Process Control 160 (2026) 103655

Contents lists available at ScienceDirect

Journal of Process Control

journal homepage: www.elsevier.com/locate/jprocont

Economic model predictive moisture control of a horizontal fluidized bed dryer for continuous pharmaceutical manufacturing

Stefan R. Tölle [a,*], Stefan Klinken-Uth [b], Ahmed Elkhashap [a], Alana Delvos [b], Heike Vallery [a], Jörg Breitkreutz [b], Sebastian Stemmler [a]

[a] Institute of Automatic Control, RWTH Aachen University, Campus-Boulevard 30, Aachen, 52074, Germany
[b] Institute of Pharmaceutics and Biopharmaceutics, Heinrich Heine University, Universitätsstr. 1, Düsseldorf, 40225, Germany

ARTICLE INFO

Keywords:
Continuous fluidized bed drying
Nonlinear model predictive control
Quality-by-control
Distributed parameter systems
Near-infrared spectroscopy

ABSTRACT

Continuous manufacturing, process analytical technology, and advanced process control are cornerstones of an ongoing effort to modernize pharmaceutical production. This paper investigates these topics in the context of horizontal fluidized bed drying in a continuous wet-granulation process. Specifically, we address the critical quality attributes residual moisture content and product temperature. The proposed nonlinear model predictive controller adjusts the residual moisture content of the drying process while limiting the product temperature. The controller is based on a semi-physical, distributed parameter model of material transport as well as heat and mass exchange in the dryer. A joint Kalman filter estimates both the process state and a model parameter describing the effectiveness of heat and mass transfer. Furthermore, a target selector minimizes the energy consumption of the process. Process analytical technology is used to continuously measure the residual moisture content. For this purpose, a partial least-squares model infers residual moisture content based on near-infrared measurements on the out-flowing product stream. The controller is validated on the lab-scale wet-granulation line QbCon® 1. The controller displays offset-free control with respect to the filtered near-infrared measurement and rise times around 3 min. The energy consumption of the QbCon® 1 was reduced by 8.8 %. The root mean square error between near-infrared and offline loss-on-drying measurements is 0.96 % moisture content. This implies that the accuracy of the controller is limited by the accuracy of the measurement.

1. Introduction

1.1. Motivation

The ability to reliably produce high-quality pharmaceutical products plays a major role in providing health care to the world population. Disruptions in the manufacturing process may result in drug shortages and recalls. For example, drug shortages reached an all-time high in the United States in early 2024 with 323 active shortages [1].

Manufacturing quality issues are a major contributor to drug shortages [2]. Despite the need for constant improvement of quality and manufacturing efficiency, the pharmaceutical industry lags behind in adopting new manufacturing paradigms in terms of automation and digitization. Traditionally, the pharmaceutical industry has been cautious about implementing these new manufacturing technologies, which may be subsumed under the term Industry 4.0 [3]. This can be explained by the high regulatory risk associated with implementing new manufacturing technologies, which includes additional validation costs and the risk of delays in the approval process.

An exemplary field of application for these new manufacturing technologies is wet granulation and drying for solid oral dosage forms. Wet granulation is a widely used technique to enlarge particles, improving flowability, blend uniformity, and compactability during tablet manufacturing. Because the process uses a granulation liquid, it requires a subsequent drying step. Both wet granulation and drying are crucial unit operations, which influence downstream processing and thus tablet quality [4]. Therefore, the produced granules are subject to stringent quality requirements. For example, the residual moisture content after the drying step is a critical quality attribute (CQA) because it influences flowability and prevents hydrolysis and the growth of mildew and bacteria [5]. Active pharmaceutical ingredient (API) degradation may also be induced through heat [6], which is of particular importance in the drying process because the granules are exposed to the high-temperature drying air. Product temperature is thus another important CQA of the drying process.

* Corresponding author.
E-mail address: s.toelle@irt.rwth-aachen.de (S.R. Tölle).

https://doi.org/10.1016/j.jprocont.2026.103655
Received 29 August 2025; Received in revised form 15 January 2026; Accepted 29 January 2026
Available online 19 February 2026

Nomenclature

Symbols

a_{PLS}	Partial least-squares model coefficient
a_{vib}	Vibration acceleration ($\mathrm{m\,s^{-2}}$)
c_{air}	Specific heat capacity of air ($\mathrm{J\,kg^{-1}\,K^{-1}}$)
D	Dispersion coefficient ($\mathrm{m^2\,s^{-1}}$)
f_{Torr}	Torricelli correction factor
g	Gravitational acceleration ($\mathrm{m\,s^{-2}}$)
h_{bed}	Fluidized bed height (m)
L	Drying bed length (m)
m_{Hup}	Dry solid hold-up mass (kg)
m_{NIR}	Calibration dataset size
$\dot{m}_{\mathrm{s}}$	Dry solid mass flow ($\mathrm{kg\,s^{-1}}$)
N	Number of spatial discretization points
N_{NIR}	Number of near-infrared sample points
NTU_{X}	Number of transfer units of mass transfer
n_{PLS}	Number of partial least-squares components
P	Process power consumption (W)
p	Model parameter
$\hat{p}$	Estimated model parameter
Δp	Drying bed pressure drop (Pa)
Q_{air}	Drying air volume flow ($\mathrm{Nm^3/s}$)
s	Slack variable
T	Granule temperature (°C)
T_0	Ambient temperature (°C)
T_{air}	Drying air temperature (°C)
T_{h}	Prediction horizon (s)
T_{s}	Sample time (s)
$\dot{T}_{\mathrm{source}}$	Temperature source term ($\mathrm{°C\,s^{-1}}$)
t, τ	Time (s)
v	Velocity ($\mathrm{m\,s^{-1}}$)
X	Dry basis moisture content
$\dot{X}_{\mathrm{sink}}$	Moisture content sink term ($\mathrm{s^{-1}}$)
Y_{air}	Drying air mixing ratio
Y_{sat}	Saturated air mixing ratio
ΔY	Air side drying potential
y	Controlled variable
y_{LOD}	Loss on drying measurement
y_{NIR}	Inferred loss on drying measurement
z	Spatial dimension (m)
Δz	Spatial discretization step size (m)
ϵ	Bed porosity
ρ_{air}	Density of air ($\mathrm{kg\,m^{-3}}$)

Vectors and Matrices

$\mathbf{0}_n$	Zero column vector with dimension n
$\tilde{\boldsymbol{A}}$	Extended system matrix
$\boldsymbol{b}_{\mathrm{PLS}}$	Partial least-squares model coefficient
$\boldsymbol{C}$	Measurement matrix
$\tilde{\boldsymbol{C}}$	Extended measurement matrix
$\boldsymbol{d}$	Measured disturbances
$\boldsymbol{I}_n$	Identity matrix of order n
$\boldsymbol{J}_{1,\dots,4}$	Jacobians
$\boldsymbol{K}$	Kalman gain
$\hat{\boldsymbol{P}}$	Estimated covariance matrix
$\boldsymbol{Q}$, R	Kalman weights
$\boldsymbol{u}$	Control variables
$\boldsymbol{W}$, W_{e}	Controller weights
$\boldsymbol{W}_\infty$, W_s	Target selector weights
$\boldsymbol{X}_{\mathrm{NIR}}$	Calibration dataset labels
$\boldsymbol{x}$	Differential state
$\hat{\boldsymbol{x}}$	Estimated state
$\tilde{\boldsymbol{x}}$	Extended state
$\boldsymbol{x}_0$	Initial state
$\boldsymbol{x}_{\mathrm{NIR}}$	Near-infrared measurement
$\boldsymbol{Y}_{\mathrm{LOD}}$	Calibration dataset features
$\boldsymbol{z}$	Algebraic states
$\hat{\boldsymbol{z}}$	Estimated algebraic states
$\boldsymbol{\Phi}$	Transition matrix
$\boldsymbol{\Omega}$	State noise matrix

Indicies

∞	Steady-state
in	Drying bed inlet
max	Maximum
min	Minimum
out	Drying bed outlet
ref	Reference

1.2. State of the art

Regulatory agencies are increasingly aware of the vast potential of the modernization of pharmaceutical manufacturing. In the past two decades, regulators have issued several guidelines to facilitate the transition. In particular, three technologies drive the modernization process:

- process analytical technology (PAT) [7–9],
- continuous manufacturing (CM) [10–12], and
- quality-by-control (QbC) [13–15].

PAT is currently the subject of extensive research in the pharmaceutical community [9]. Most commonly, a CQA is not measured directly but inferred through spectroscopy. Hence, a mathematical model is needed to relate the measured spectrum to the physical, chemical, or biological attribute of interest. Other approaches include tomography and image analysis. The final aim of the PAT concept would be the real-time release-testing of the drug product, i.e., evaluating product quality during process operation.

The advantages of CM in terms of cost, flexibility, and product quality are well known in the chemical and food industry. Advantages of particular importance for the pharmaceutical industry are the easier scale-up, the reduction in stockpiles, and the potential for high-quality consistency [16]. For example, the easier scale-up reduces the cost-critical time to market and reduced stockpiles are beneficial for medicines subject to expiration. A major milestone for the adoption of CM in pharmaceutical manufacturing was the FDA's approval of Orkambi in 2015, which is the first oral solid dosage form produced using a continuous manufacturing process.

CM also favors process automation, due to the tight integration of individual unit operations. Combined with PAT, CM is well suited for closed-loop control of CQAs [14]. However, CM also introduces new challenges in regard to system modeling and control. Spatially distributed continuous processes are usually described using partial differential equations (PDEs). However, most methods from control

theory rely on a description of the system through ordinary differential equations (ODEs). Another difficulty is that the material flow can often not be modeled solely from first principles. Typically, material flow is characterized by a residence time distribution (RTD). A model for the residence time enables compliance with regulations on material tracing [10]. The residence time model additionally characterizes the system dynamics.

QbC goes beyond the traditional quality-by-testing, which involves extensive tests on the final product. Conventionally, quality-by-testing is a consequence of a lack of knowledge of the relationship between critical process parameters (CPPs) and final product quality. Therefore, it keeps CPPs and critical material attributes (CMAs) in a tightly constrained range. If quality tests fail, the whole batch is discarded, leading to excessive waste. Another disadvantage of this approach is that the usually destructive quality tests preclude full test coverage. Since deficient quality often only occurs in a small percentage of the produced medicine, this can pose a serious risk to the patient.

The quality-by-design (QbD) initiative [17] tries to mitigate this risk by drawing upon enhanced process understanding. Central to the QbD concept is the definition of a design space. The design space is the space of CPPs and CMAs for which it can be guaranteed that the CQA specifications are met. If the regulatory authority approves the design space, the process can be operated within the design space. This way, testing can be reduced, although end-product testing — for instance, for batch release — continues to take place.

The QbC concept goes yet another step further than the QbD approach [14]. QbC describes the closed-loop control of CQAs. By operating the controller within the design space, regulatory compliance is assured and product quality can be further improved. Nevertheless, QbC is still not yet implemented in most parts of pharmaceutical manufacturing [18]. This is mainly due to insufficient real-time monitoring of the CQAs through PAT.

In the case of wet granulation and drying, the CQAs of interest include the particle size, residual moisture content, granule strength, granule content uniformity, and granule temperature. Of these, the drying process mainly influences the residual moisture content and the granule temperature [19].

So far, most research on closed-loop control of fluidized bed drying has focused on batch processes [20–22]. Only few contributions [23–25] describe closed-loop control of continuous horizontal fluidized bed dryers. For example, [25] describes a model predictive controller (MPC) and derives a linear model from input–output data of a tank-in-series nonlinear model. The controller also considers the energy consumption of the process. These contributions were theoretically focused and did not yet include experimental validation of the controller. In addition, they all rely on a linear model, which is derived from a simulation of the dryer, to formulate the control problem. However, the drying process has considerable nonlinearities due to the two drying stages [26].

1.3. Contribution and scope

In this contribution, we design and experimentally evaluate a NMPC for a continuous horizontal fluidized bed dryer, namely the lab-scale production unit QbCon® 1 (L.B. Bohle Maschinen+Verfahren GmbH, Ennigerloh, Germany) [27]. Although the wet granulation process has many more CQAs, e.g., granule size distribution, we limit ourselves in this contribution to granule drying and thus only investigate granule moisture content and temperature. The process parameters of the granulator are not adapted by our proposed controller. Hence, the granulation CQAs are excluded in this work but could be addressed with a separate controller. The separation of unit operations greatly reduces overall system complexity. Interactions between unit operations are considered disturbances to the individual controllers in this approach.

In contrast to existing linear controllers of the continuous drying process, we choose the more general approach of directly using a physical nonlinear drying model in the formulation of the MPC.

Our group published a first proof-of-concept of the NMPC control approach in [28], already featuring:

1. offset free control of the (filtered) residual moisture content,
2. validity for different operating points,
3. physical insight through a physical model structure, and
4. an observer allowing for process monitoring.

This paper extends the previous work mainly by extensive experimental validation, but also with a few methodological improvements:

5. limitation of the product temperature to avoid API degradation,
6. minimization of the energy consumption,
7. online model parameter adaptation to account for different product formulations.

2. Modeling

2.1. Continuous drying model

The dryer of the QbCon® 1 is a horizontal vibrated fluidized bed dryer (VFBD). A schematic is shown in Fig. 1. Granules enter the VFBD after twin-screw wet granulation with an initial moisture content X_{in}. They are transported through the fluidized drying bed with length L along the spatial dimension z by an asymmetric vibration of the distributor plate with vibration acceleration a_{vib}. Drying air flows perpendicular to the direction of granule transport. Lower-level PID controllers track the reference drying air temperature T_{air}, drying air volume flow Q_{air}, and vibration acceleration a_{vib}.

In previous work, we developed a gray-box model that describes the VFBD [26,29]. The modeling assumptions made therein are quite general, such that the model would potentially also apply to larger production units. The model consists of a white-box and a black-box part. The white-box part describes the interaction between particles and drying air in an adiabatic humidification process. The black-box part is a Gaussian process model (GPM) that estimates the parameters of the particle transport dynamics [30]. This is done because modeling particle transport from first principles alone is computationally intractable. Both model parts are combined to predict the granule dry-basis moisture content $X(z,t)$ and the granule temperature $T(z,t)$ through two PDEs:

$$\frac{\partial X}{\partial t} = -v\frac{\partial X}{\partial z} + D\frac{\partial^2 X}{\partial z^2} - \dot{X}_{\text{sink}}, \tag{1a}$$

$$\frac{\partial T}{\partial t} = -v\frac{\partial T}{\partial z} + D\frac{\partial^2 T}{\partial z^2} + \dot{T}_{\text{source}}, \tag{1b}$$

with the corresponding boundary conditions

$$X(t,0) = X_{\text{in}}, \quad \left.\frac{\partial X}{\partial z}\right|_{z=L} = 0, \tag{2a}$$

$$T(t,0) = T_{\text{in}}, \quad \left.\frac{\partial T}{\partial z}\right|_{z=L} = 0. \tag{2b}$$

This corresponds to two axial dispersion models with interacting source/sink terms. The source term $\dot{T}_{\text{source}}$ and the sink term $\dot{X}_{\text{sink}}$ respectively model the heat and mass exchange between granules and drying air. The term $\dot{T}_{\text{source}}$ depends on $\dot{X}_{\text{sink}}$ due to the dependence of the heat of evaporation on the drying rate. The boundary conditions for $z = 0$ are given by the known inlet moisture content X_{in} and inlet temperature T_{in}.

The number of transfer units NTU_{X} of mass transfer is a dimensionless parameter that describes the effectiveness of mass transfer between granules and drying air. Since mass and heat transfer are related through the Lewis number, NTU_{X} also affects the rate of heat transfer. The parameter NTU_{X} thus encodes various physical parameters associated with heat and mass transfer, such as the unknown mass and heat transfer coefficients. The variable NTU_{X} is treated as a tuning parameter of the model (see [26] for details on fitting and validation). It may change if a different material is being dried.

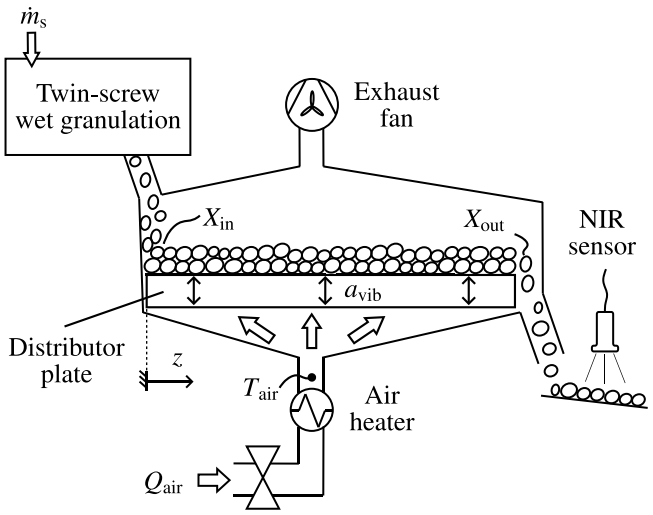

Fig. 1. Schematic of the vibrated fluidized bed dryer under investigation.
Source: Adapted from [29].

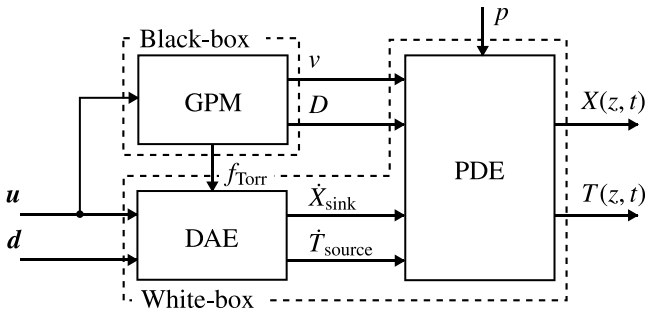

Fig. 2. Structure of the gray-box drying model.
Source: Adapted from [32].

The model structure is summarized in Fig. 2. The GPM estimates the velocity v and the dispersion coefficient D of the particle transport. These parameters depend on the process parameters a_{vib} and Q_{air}, which are the inputs of the GPM. Labeled training data is collected from tracer experiments. The collected training data covers the entire design space of the process parameters, such that the GPM does not have to extrapolate the data. For more details, including model formulation, data generation, and model validation, the reader is referred to [30].

Finally, a system of differential algebraic equations (DAEs) models the dry solid hold-up mass m_{Hup} and the air-side drying potential ΔY, which are needed to formulate the source/sink terms in (1):

$$\dot{m}_{Hup} = \dot{m}_{s,in} - \underbrace{f_{Torr}\frac{m_{Hup}}{L}\sqrt{2gh_{bed}}}_{\dot{m}_{s,out}}, \tag{3}$$

$$0 = g_1(\varepsilon, \Delta p, m_{Hup}, Q_{air}), \tag{4}$$

$$0 = g_2(T_{sat}, T_{air}, Y_{air}). \tag{5}$$

Eq. (3) models the dry solid hold-up mass m_{Hup} by a lumped parameter mass balance. To reduce model complexity, the dependency of the hold-up mass on the spatial coordinate z is neglected. The Torricelli correction factor f_{Torr} is predicted by a GPM, which is trained on hold-up mass measurements. The inlet mass flow rate $\dot{m}_{s,in}$ is controlled by a lower-level PID controller. The bed height h_{bed} is calculated from the bed porosity ε. The bed porosity is given implicitly by (4) from the Ergun formula as a function of the pressure drop Δp across the bed [29].

To obtain the air-side drying potential $\Delta Y = Y_{sat} - Y_{air}$, the drying air mixing ratio Y_{air} is measured. The mixing ratio Y_{sat} and temperature T_{sat} at the saturation point are calculated implicitly by finding the intersection of the fog isotherm with the saturation line in the Mollier h-Y-Diagram [31]. This can be represented by the algebraic relation (5).

The described model is able to predict the granule temperature ($RMSE = 4\,\mathrm{K}$) and residual moisture content ($RMSE = 0.021$) with sufficient accuracy for control applications [26]. Influencing factors like material attributes and environmental conditions are so far not taken into account. We will address these sources of variability later with an online model adaptation scheme.

2.2. Discretization

As a prerequisite for control and state estimation, the model is discretized and brought into nonlinear state-space form. Specifically, Eq. (1a) is discretized using the method of lines on a uniform N point spatial grid with segment length

$$\Delta z = \frac{L}{N+1}. \tag{6}$$

The following vectors are defined summarizing differential states $\boldsymbol{x} \in \mathbb{R}^{N+1}$, algebraic variables $\boldsymbol{z} \in \mathbb{R}^2$, control variables $\boldsymbol{u} \in \mathbb{R}^3$, measured disturbances $\boldsymbol{d} \in \mathbb{R}^5$ and the model parameter $p \in \mathbb{R}$:

$$\boldsymbol{x} := [X(t, \Delta z), X(t, 2\Delta z), \dots, X(t, L-\Delta z), m_{Hup}]^T, \tag{7}$$

$$\boldsymbol{z} := [\varepsilon, T_{sat}]^T, \tag{8}$$

$$\boldsymbol{u} := [Q_{air}, T_{air}, a_{vib}]^T, \tag{9}$$

$$\boldsymbol{d} := [Y_{air}, \Delta p, X_{in}, T_{in}, \dot{m}_{s,in}]^T, \tag{10}$$

$$p := NTU_X. \tag{11}$$

Even though the inlet moisture content X_{in} and the solid mass flow $\dot{m}_{s,in}$ can be manipulated through lower-level controllers, they are not treated as control variables of the higher-level moisture controller. These degrees of freedom can instead be utilized to achieve other objectives. For example, the inlet moisture content is well suited to control the particle size [33] and the solid mass flow may be used to synchronize the throughput with other unit operations.

The convection term of (1a) is discretized using first-order backward differences (upwind)

$$\left.\frac{\partial X}{\partial z}\right|_{z^*} \approx \frac{X(z^*) - X(z^* - \Delta z)}{\Delta z} \tag{12}$$

and the diffusion term using second-order central differences:

$$\left.\frac{\partial^2 X}{\partial z^2}\right|_{z^*} \approx \frac{X(z^* + \Delta z) - 2X(z^*) + X(z^* - \Delta z)}{\Delta z^2}. \tag{13}$$

The boundary conditions (2a) are implemented using the ghost point method [28]. In the ghost point method, the boundary conditions are evaluated to derive expressions for the moisture content on the left and right boundaries. Namely, we get:

$$X(0) = X_{in} \tag{14}$$

$$\frac{X(L) - X(L-\Delta z)}{\Delta z} = 0 \Rightarrow X(L) = X(L-\Delta z) \tag{15}$$

The discretized model can be written as a system of DAEs in semi-explicit form, as follows:

$$\dot{\boldsymbol{x}} = \boldsymbol{f}(\boldsymbol{x}, \boldsymbol{z}, \boldsymbol{u}, \boldsymbol{d}, p), \tag{16a}$$

$$\boldsymbol{0}_2 = \boldsymbol{g}(\boldsymbol{x}, \boldsymbol{z}, \boldsymbol{u}, \boldsymbol{d}), \tag{16b}$$

$$y = \boldsymbol{C}\boldsymbol{x}, \tag{16c}$$

with the measurement matrix

$$\boldsymbol{C} := [\underbrace{0, \dots, 0}_{(N-1)\text{-times}}, 1, 0] \tag{17}$$

and the system output $y := X_{out}$.

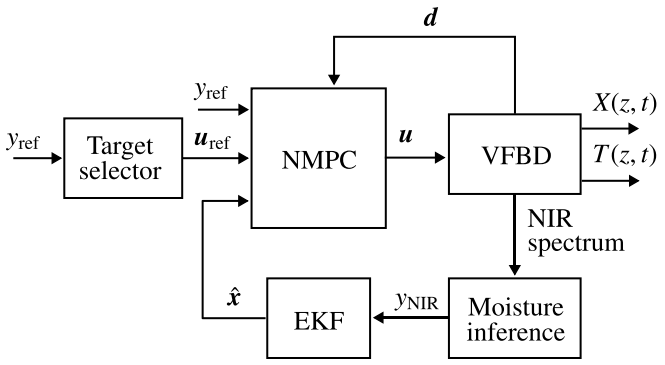

Fig. 3. Block diagram of the presented control scheme.

3. Control scheme

3.1. Approach

Fig. 3 depicts the block diagram of the proposed control scheme. The system output y, i.e., the residual moisture content, is inferred from the NIR spectrum measured at the VFBD outlet (see Fig. 1). To reconstruct the moisture content along the whole drying bed, an EKF is employed. The EKF also implements the online parameter adaptation to account for different product formulations.

The NMPC controls the residual moisture content based on the estimated state $\hat{\boldsymbol{x}}$ and the measured disturbances $\boldsymbol{d}$. Since the system is overactuated, the control loop also features a target selector. The target selector aims to minimize the energy consumption of the process.

All components of the control scheme are evaluated at the discrete time steps $t_k = k \cdot T_s$ with the sample time T_s. A detailed description of the individual components is given in the following sections.

3.2. State and parameter estimation

The only measurements available on the experimental setup are the residual moisture content $y = X_{out}$ and the measured disturbances $\boldsymbol{d}$. In order to apply NMPC, the whole state space vector $\boldsymbol{x}$ needs to be known or approximated. Therefore, an EKF was designed for model (16) to recover full state information, in particular, the moisture content within the drying bed.

Special care must be taken to account for the algebraic constraints (16b). For this, we use the algorithm proposed in [34]. Since (16) is an index-1 DAE, linearization yields

$$\dot{\boldsymbol{x}} = \boldsymbol{J}_1 \boldsymbol{x} + \boldsymbol{J}_2 \boldsymbol{z}, \tag{18a}$$

$$\boldsymbol{0}_2 = \boldsymbol{J}_3 \boldsymbol{x} + \boldsymbol{J}_4 \boldsymbol{z}, \tag{18b}$$

with the Jacobians

$$\begin{aligned} \boldsymbol{J}_1 &= \frac{\partial \boldsymbol{f}}{\partial \boldsymbol{x}} \in \mathbb{R}^{(N+1)\times(N+1)}, & \boldsymbol{J}_2 &= \frac{\partial \boldsymbol{f}}{\partial \boldsymbol{z}} \in \mathbb{R}^{(N+1)\times 2}, \\ \boldsymbol{J}_3 &= \frac{\partial \boldsymbol{g}}{\partial \boldsymbol{x}} \in \mathbb{R}^{2\times(N+1)}, & \boldsymbol{J}_4 &= \frac{\partial \boldsymbol{g}}{\partial \boldsymbol{z}} \in \mathbb{R}^{2\times 2}. \end{aligned} \tag{19}$$

Differentiating (18b) converts the algebraic constraint into the ODE:

$$\dot{\boldsymbol{z}} = -\boldsymbol{J}_4^{-1}\boldsymbol{J}_3\boldsymbol{J}_1\boldsymbol{x} - \boldsymbol{J}_4^{-1}\boldsymbol{J}_3\boldsymbol{J}_2\boldsymbol{z}. \tag{20}$$

Hence, the algebraic variables can be treated as differential states in an extended state space.

The model tuning parameter p is not fitted to offline measurements, but estimated online. The EKF jointly estimates the states and the parameter with sample time T_s (joint EKF). This way, the model can adapt, for example, to changing material properties. The usual approach to achieve offset-free model predictive control despite model mismatch is the estimation of a constant output disturbance. In the presented case, this is made superfluous by the estimation of p. In steady state, the joint Kalman filter will adjust the model parameter until the model's prediction matches the measurement. Hence, by using the estimated parameter value, the NMPC can achieve offset-free control. The advantage of parameter estimation over the estimation of an output disturbance is that the model retains its physical structure. The parameter estimate $\hat{p}$ can be physically interpreted and may be used for process monitoring. A possible alternative to the here used joint EKF is the dual EKF, which uses two EKFs for parameter and state estimation. This may reduce computational complexity but ignores the cross-covariance between the parameter and the states [35].

The extended state vector

$$\tilde{\boldsymbol{x}} := \left[\boldsymbol{x}^\mathrm{T},\ p,\ \boldsymbol{z}^\mathrm{T}\right]^\mathrm{T} \tag{21}$$

consists of the differential states $\boldsymbol{x}$, the model parameter p, and the algebraic states $\boldsymbol{z}$. Since the model parameter p is unknown, its dynamic equation is assumed to follow a random walk with no deterministic differential component, i.e., $\dot{p} = 0$.

Together with (18a) and (20), the linearized joint state-space model is:

$$\dot{\tilde{\boldsymbol{x}}} = \tilde{\boldsymbol{A}}\tilde{\boldsymbol{x}} \tag{22a}$$

$$y = \tilde{\boldsymbol{C}}\tilde{\boldsymbol{x}} \tag{22b}$$

$$\text{with } \tilde{\boldsymbol{A}} := \begin{bmatrix} \boldsymbol{J}_1 & \boldsymbol{0}_{N+1} & \boldsymbol{J}_2 \\ \boldsymbol{0}_{N+1}^\mathrm{T} & 0 & \boldsymbol{0}_2^\mathrm{T} \\ -\boldsymbol{J}_4^{-1}\boldsymbol{J}_3\boldsymbol{J}_1 & \boldsymbol{0}_2 & -\boldsymbol{J}_4^{-1}\boldsymbol{J}_3\boldsymbol{J}_2 \end{bmatrix},$$

$$\tilde{\boldsymbol{C}} := \begin{bmatrix} \boldsymbol{C} & 0 & 0 & 0 \end{bmatrix}.$$

For state estimation, the measurement y is assumed to be subject to measurement white noise with known variance R. White noise is considered for the differential states $\boldsymbol{x}$ and the model parameter p but not for the algebraic states $\boldsymbol{z}$. We assume that the state noise covariance matrix $\boldsymbol{Q} \in \mathbb{R}^{(N+2)\times(N+2)}$ of the joint state space $[\boldsymbol{x}^\mathrm{T},\ p]^\mathrm{T}$ is known as well. In this case, the state noise covariance matrix $\boldsymbol{\Omega}$ of the extended state space can be calculated according to [34]:

$$\boldsymbol{\Omega} = \boldsymbol{\Gamma}\boldsymbol{Q}\boldsymbol{\Gamma}^\mathrm{T} \tag{23}$$

$$\text{with } \boldsymbol{\Gamma} = \begin{bmatrix} \boldsymbol{I}_{N+2} \\ -\boldsymbol{J}_4^{-1}[\boldsymbol{J}_3 \quad \boldsymbol{0}_2] \end{bmatrix}.$$

The EKF algorithm for time step t_k is summarized below. The algorithm is adapted from [32].

Algorithm 1: Joint EKF with algebraic states

Input: $\hat{\boldsymbol{x}}_{k-1}$, $\hat{\boldsymbol{P}}_{k-1}$, $\hat{\boldsymbol{z}}_{k-1}$, $\boldsymbol{u}_{k-1}$, $\boldsymbol{d}_{k-1}$, y_k, $\boldsymbol{Q}$, R
Output: $\hat{\boldsymbol{x}}_k$, $\hat{\boldsymbol{P}}_k$, $\hat{\boldsymbol{z}}_k$

1 $\hat{\boldsymbol{x}}_k$ = integration step of (16) ▷ Prediction
2 Evaluate $\boldsymbol{J}_{1,\dots,4}$ at $\hat{\boldsymbol{x}}_{k-1}$, $\hat{\boldsymbol{z}}_{k-1}$, $\boldsymbol{u}_{k-1}$, $\boldsymbol{d}_{k-1}$ ▷ Jacobians
3 $\boldsymbol{\Phi} = \exp\left(\tilde{\boldsymbol{A}}T_s\right)$ ▷ Transition matrix
4 $\hat{\boldsymbol{P}}_k = \boldsymbol{\Phi}\hat{\boldsymbol{P}}_{k-1}\boldsymbol{\Phi}^\mathrm{T} + \boldsymbol{\Gamma}\boldsymbol{Q}\boldsymbol{\Gamma}^\mathrm{T}$ ▷ Covariance propagation
5 $\boldsymbol{K}_k = \hat{\boldsymbol{P}}_k\tilde{\boldsymbol{C}}\left(\tilde{\boldsymbol{C}}\hat{\boldsymbol{P}}_k\tilde{\boldsymbol{C}}^\mathrm{T} + R\right)^{-1}$ ▷ Kalman gain
6 $\hat{\boldsymbol{x}}_k \leftarrow \hat{\boldsymbol{x}}_k + \boldsymbol{K}\left(y - \tilde{\boldsymbol{C}}\hat{\boldsymbol{x}}_k\right)$ ▷ State correction
7 $\hat{\boldsymbol{P}}_k \leftarrow \left(\boldsymbol{I} - \boldsymbol{K}\tilde{\boldsymbol{C}}\right)\hat{\boldsymbol{P}}_k$ ▷ Covariance correction
8 $\hat{\boldsymbol{z}}_k$ = roots of $\boldsymbol{g}(\cdot)$ at $\hat{\boldsymbol{x}}_k, \boldsymbol{u}_{k-1}, \boldsymbol{d}_{k-1}$ ▷ Reconcile algebraic states

3.3. Nonlinear model predictive control

The NMPC scheme leverages the above-described drying model explicitly for control. This aligns well with the QbC principle of utilizing process knowledge to control the process. The approach also allows the formulation of constraints to ensure safe operation. Here, constraints restrict the control variables to remain inside the design space and the product temperature to prevent heat-induced API degradation.

The controller receives measurements of the disturbances $\boldsymbol{d}$ before each evaluation step. Furthermore, the EKF provides a current estimate of the parameter p. The dependence of the algorithm on $\boldsymbol{d}$ and p is thus omitted in the following section.

In each time step t_k, the NMPC solves the following optimal control problem:

$$\min_{\boldsymbol{x}(\cdot),y(\cdot),\boldsymbol{z}(\cdot),\boldsymbol{u}(\cdot),s(\cdot)} \underbrace{\int_{t_k}^{t_k+T_\mathrm{h}} \frac{1}{2} \left\| \begin{bmatrix} y_\mathrm{ref} - \boldsymbol{C}\boldsymbol{x}(\tau) \\ \boldsymbol{u}_\mathrm{ref} - \boldsymbol{u}(\tau) \\ \dot{\boldsymbol{u}}(\tau) \\ s(\tau) \end{bmatrix} \right\|_{\boldsymbol{W}}^2 \mathrm{d}\tau}_{\text{Stage cost}} + \underbrace{\frac{1}{2} W_\mathrm{e} \left(y_\mathrm{ref} - \boldsymbol{C}\boldsymbol{x}(T_\mathrm{h}) \right)^2}_{\text{Terminal cost}}, \tag{24a}$$

$$\text{s.t.} \quad \boldsymbol{x}(0) = \boldsymbol{x}_0, \tag{24b}$$

$$\dot{\boldsymbol{x}} = \boldsymbol{f}(\boldsymbol{x}, \boldsymbol{z}, \boldsymbol{u}, \boldsymbol{d}, p), \tag{24c}$$

$$\boldsymbol{0}_2 = \boldsymbol{g}(\boldsymbol{x}, \boldsymbol{z}, \boldsymbol{u}, \boldsymbol{d}), \tag{24d}$$

$$\boldsymbol{u}_\mathrm{min} \le \boldsymbol{u} \le \boldsymbol{u}_\mathrm{max}, \tag{24e}$$

$$T_\infty(\boldsymbol{u}(\tau))|_{z=L} - s(\tau) \le T_\mathrm{max}, \tag{24f}$$

$$s(\tau) \ge 0. \tag{24g}$$

The controller minimizes the deviation from the desired residual moisture content y_ref over the prediction horizon T_h. Due to the parameter estimation scheme, as detailed in Section 3.2, a consideration of steady-state model errors is not necessary at this point. Further stage costs arise from the deviation of the control variable from a desired set-point $\boldsymbol{u}_\mathrm{ref}$ and by the rate of change $\dot{\boldsymbol{u}}$ of the control variable. The desired set-point $\boldsymbol{u}_\mathrm{ref}$ is chosen by a target selector as elaborated later in Section 3.4. Since the process model does not include any actor dynamics, the costs associated with $\dot{\boldsymbol{u}}$ must be chosen such that the resulting trajectory of $\boldsymbol{u}$ is feasible. The individual terms of the stage cost are weighted with the positive semidefinite tuning matrix $\boldsymbol{W} \in \mathbb{R}^{8\times8}$. The terminal cost term considers the deviation of the residual moisture content from the reference at the end of the prediction horizon. The terminal cost is weighted with the tuning parameter W_e.

The optimal control problem (24) is subject to the initial state $\boldsymbol{x}_0$, which is the current state estimate of the EKF, and to the model Eqs. (16). The constraint (24e) limits the operating range of the controller. The minimum and maximum values of the control variables are given by $\boldsymbol{u}_\mathrm{min}$ and $\boldsymbol{u}_\mathrm{max}$, respectively. This constraint can be used to address actuator limits. Additionally, the controller can be restricted to only operate within the design space of the process. This presents a tighter restriction of the control variables than the limitations given by the actuators, but it enables regulatory compliance.

Lastly, the controller considers the granule temperature. With the presented methods, a simultaneous control of residual moisture content and temperature, i.e., $\boldsymbol{y} = [X_\mathrm{out}, T_\mathrm{out}]^\mathrm{T}$, would be feasible. For this, (1b) must be discretized in the same way as (1a) and the discretized temperature states must be added to the state space. From a quality standpoint however, it is enough to keep the temperature below a certain maximum temperature T_max. Hence, the controller only considers the granule temperature in the form of a constraint.

If the temperature model is discretized and the model's state space is extended accordingly, limiting the granule temperature would correspond to a linear state constraint. This approach is computationally expensive, since the number of decision variables would increase by the number of discretization points N. Instead, for the presented use case, a steady-state consideration will suffice. The idea is to constrain the control variables to those inputs that would result in permissible steady-state temperatures. This corresponds to a nonlinear constraint on $\boldsymbol{u}$ because the maximum steady-state temperature is only a function of the process variables. During steady-state conditions, the two PDEs given by (1) reduce to ODEs. The steady-state moisture content $X_\infty(z)$ and temperature $T_\infty(z)$ is the solution to the following boundary value problem (BVP):

$$0 = -v\frac{\mathrm{d}X_\infty}{\mathrm{d}z} + D\frac{\mathrm{d}^2X_\infty}{\mathrm{d}z^2} - \dot{X}_\mathrm{sink}, \quad z \in [0, L], \tag{25a}$$

$$0 = -v\frac{\mathrm{d}T_\infty}{\mathrm{d}z} + D\frac{\mathrm{d}^2T_\infty}{\mathrm{d}z^2} + \dot{T}_\mathrm{source}, \tag{25b}$$

$$X_\infty(0) = X_\mathrm{in}, \quad \left.\frac{\mathrm{d}X_\infty}{\mathrm{d}z}\right|_{z=L} = 0, \tag{25c}$$

$$T_\infty(0) = T_\mathrm{in}, \quad \left.\frac{\mathrm{d}T_\infty}{\mathrm{d}z}\right|_{z=L} = 0. \tag{25d}$$

We address the BVP through finite differences, discretizing the differential equation over the spatial domain with (12) and (13), and then applying Newton's method to solve the resulting system of nonlinear equations. We expect the highest granule temperature at the bed outlet and therefore choose the last discretization point of the steady-state temperature T_∞ for (24f). The slack variable s guarantees feasibility of this temperature constraint.

3.4. Target selection

The drying air temperature T_air, the drying air volume flow Q_air, and the vibration acceleration a_vib all influence the residual moisture content X_out. Hence, with three inputs and only one controlled variable, the system (16) is over-actuated. For this reason, [28] proposed a target selector that keeps the steady-state inputs close to desired reference values $\boldsymbol{u}_\mathrm{des}$. In the above-described framework, this reference target selector can be described by the following nonlinear program:

$$\boldsymbol{u}_\mathrm{ref} = \arg\min_{\boldsymbol{u},s} \ \|\boldsymbol{u} - \boldsymbol{u}_\mathrm{des}\|_{\boldsymbol{W}_\infty}^2 + W_s s^2, \tag{26a}$$

$$\text{s.t.} \quad \boldsymbol{u}_\mathrm{min} \le \boldsymbol{u} \le \boldsymbol{u}_\mathrm{max}, \tag{26b}$$

$$X_\infty(\boldsymbol{u})|_{z=L} + s = y_\mathrm{ref}, \tag{26c}$$

$$T_\infty(\boldsymbol{u})|_{z=L} \le T_\mathrm{max}, \tag{26d}$$

weighting matrices $\boldsymbol{W}_\infty$ and W_s and the slack variable s.

In this paper, we use a different target selector formulation, which we will call economic target selector. The economic target selector utilizes the additional degrees of freedom to minimize the energy consumption of the process. We assume that the influence of the control inputs on the energy consumption is determined by the energy needed to heat up the drying air. The energy costs associated with blowing and vibration are subsequently neglected. The power consumption is thus given by:

$$P = P_\mathrm{const} + Q_\mathrm{air}\rho_\mathrm{air}c_\mathrm{air}(T_\mathrm{air} - T_0), \tag{27}$$

with the air density ρ_air, specific heat capacity c_air, ambient temperature T_0, and the constant power consumption P_const.

The economic control objective can either be approached by adding an additional cost term to the optimal control problem (24) of the NMPC or by calculating a target $\boldsymbol{u}_\mathrm{ref}$ for the control variables [25]. In the first case, the cost function in (24a) loses its nonlinear least squares form. This comes with a substantial computational burden because a computationally cheap approximation of the Hessian using Gauss–Newton-type methods is no longer available. The Hessian is then usually computed exactly [36]. To avoid this, the economic cost is instead minimized with a target selector. This approach decouples the economic and dynamical objectives, which may lead to suboptimal solutions. However, in practice, the process is operated in steady state for the vast majority of the time. Since the target selector and the NMPC have the same underlying model, under steady state conditions, the penalty term $(\boldsymbol{u}_\mathrm{ref} - \boldsymbol{u})$ vanishes. That means that in steady state, the economic and dynamic objectives do not conflict with each other, and the process is operated optimally. Furthermore, the comparative

Table 1
Tuning parameters of the control scheme.

	Symbol	Description	Value
General	T_s	Sample time	1 s
	N	Number of spatial discretization points	15
	T_{max}	Maximum granule temperature	45 °C
	$\boldsymbol{u}_{min}$	Minimum control variables	$[5\,Nm^3h^{-1},\ 40\,°C,\ 6\,ms^{-2}]^T$
	$\boldsymbol{u}_{max}$	Maximum control variables	$[30\,Nm^3h^{-1},\ 90\,°C,\ 10\,ms^{-2}]^T$
EKF	$\boldsymbol{Q}$	State noise covariance matrix	diag(0.1; … ; 0.1; 10)
	R	Measurement noise variance	500
NMPC	$\boldsymbol{W}$	Stage cost weight	diag(30; 0.04; 0.001; 0.01; 0.4; 0.01; 1; 1)
	W_e	Terminal cost weight	100
	T_h	Prediction horizon	60 s
Ref. target selector	$\boldsymbol{W}_\infty$	Target selector weight	$\mathrm{diag}(0.0016\,Nm^{-6}h^2; 0.0004\,K^{-2}; 0.0625\,m^{-2}s^4)$
	W_s	Slack variable weight	10^9
	$\boldsymbol{u}_{des}$	Desired control inputs	$[17.5\,Nm^3h^{-1},\ 65\,°C,\ 8\,ms^{-2}]$
Econ. target selector	W_s	Slack variable weight	10^9

study [25] provides strong empirical support for the effectiveness of a two-stage approach for the presented use case.

The target $\boldsymbol{u}_{ref}$ of the economic target selector is the solution of the following nonlinear program:

$$\boldsymbol{u}_{ref} = \arg\min_{\boldsymbol{u},s} \; Q_{air}\left(T_{air} - T_0\right) + W_s s^2, \tag{28a}$$

$$\text{s.t.} \quad \boldsymbol{u}_{min} \le \boldsymbol{u} \le \boldsymbol{u}_{max}, \tag{28b}$$

$$X_\infty(\boldsymbol{u})\big|_{z=L} + s = y_{ref}, \tag{28c}$$

$$T_\infty(\boldsymbol{u})\big|_{z=L} \le T_{max}. \tag{28d}$$

The first term in (28a) is derived from the power demand (27). The second term penalizes the slack variable s introduced in (28c). With the slack variable, the optimization problem retains feasibility even if an unattainable output reference y_{ref} is chosen. The weight W_s should be sufficiently large to reach negligible deviations from the reference y_{ref} during normal operation. Eq. (28d) ensures that the result of the optimization is feasible for the optimal control problem (24). The steady-state functions X_∞ and T_∞ are calculated from the BVP as described in the previous section. Hence, $\boldsymbol{u}_{ref}$ is the optimal feasible input that achieves the desired output y_{ref} in steady-state while minimizing the energy consumption.

3.5. Implementation

We implemented the model in MATLAB using the MATLAB interface of the open-source software package CasADi [37]. The software allows the symbolic definition and algorithmic differentiation of the model equations described in Section 2. The SUNDIALS suite [38,39] is distributed along with CasADi. It provides the solver IDAS for DAEs that is used to integrate (16). Casadi employs Ipopt [40] for solving the nonlinear program (28). Additionally, CasADi can solve systems of nonlinear equations using Newton's method. This functionality is employed to solve the BVP (25). Crucially, the resulting expression remains differentiable and can therefore be used as a nonlinear constraint in (24) and (28). The optimal control problem (24) is solved using the open-source software package acados [41], which can directly use the model formulated in CasADi.

Table 1 summarizes the main tuning parameters of the control scheme. Preliminary tests showed that fifteen spatial discretization points lead to discretization errors that are one order of magnitude smaller than the modeling errors observed in [26]. Hence, it was decided that fifteen spatial discretization points suffice. Since no API was used in the drying experiments, the maximum allowable product temperature T_{max} cannot be derived. For demonstration purposes, we chose the maximum product temperature T_{max} such that intensive drying conditions trigger the temperature constraint. The limits of the process parameters $\boldsymbol{u}_{min}$ and $\boldsymbol{u}_{max}$ were chosen based on actuator limits and on drying performance. For example, the minimum vibration acceleration is set to $6\,ms^{-2}$ because this value prevents granules from getting stuck in the VFBD.

We chose the prediction horizon T_h larger than the mean residence time to capture the relevant system dynamics, and we manually tuned the weighting matrices of the EKF and the NMPC based on initial experimentation. The measurement noise variance $R = 500$ achieves good noise rejection. The entry in the covariance matrix $\boldsymbol{Q}$ corresponding to the model parameter p is tuned separately, such that $\hat{p}$ changes more slowly than the dynamic system states. As mentioned above, the stage cost $\boldsymbol{W}$ is tuned to produce references for the process parameters that are realizable for the lower level PID controllers. For this, we tuned the entries corresponding to the individual control inputs separately.

To initialize the EKF, the initial moisture content along the drying bed is approximated by exponential decay:

$$X(t=0,z) \approx X_{in}\exp\left(-3z/L\right). \tag{29}$$

The initial covariance matrix $\hat{\boldsymbol{P}}_0$ is chosen to be the identity matrix.

The reference target selector is parametrized to keep the control inputs in the center of the operating region, i.e., $\boldsymbol{u}_{des} = (\boldsymbol{u}_{max} + \boldsymbol{u}_{min})/2$. The weighting matrix $\boldsymbol{W}_\infty$ normalizes the control variables such that each deviation from the desired control inputs is weighted equally: $\boldsymbol{W}_{\infty,ii} = 1/(u_{max,i} - u_{min,i})^2$.

4. Inline moisture content inference

As stated before, a key challenge with closed-loop moisture control is the continuous in-line measurement of the controlled variable. Conventional approaches to measuring moisture contents, such as LOD and Karl Fischer titration, only provide an at-line measurement of a drawn sample. NIR spectroscopy for moisture content inference is an alternative that can provide continuous measurement signals since water has strong absorption bands in the NIR region. NIR spectroscopy for inline sensing is an active and still developing research area [42–44].

Fig. 4 depicts the measurement setup for the closed-loop control, which includes a commercial NIR spectrometer (Raspberry spegg© NIR22, Dr. Licht GmbH, Nümbrecht, Germany). The software for moisture content inference was written by the authors. To improve the signal-to-noise ratio, the spectrometer was cooled using pressurized air. The NIR spectrum was measured reflectively on the out-flowing product stream. To ensure sufficiently strong illumination in the wavelength range, a halogen lamp operating at approximately 25 W was used. Compressed air was used to prevent dust accumulation and charring on the lamp. The NIR spectrum in the range 1100–1600 nm was sampled with a resolution of 6 nm, which results in $N_{NIR} = 84$ sample points. The spectrometer is connected to a Raspberry Pi, which sends the measured spectra to a lab PC for further processing.

A mathematical model is necessary to infer the residual moisture content from the NIR measurement. A NIR calibration dataset was

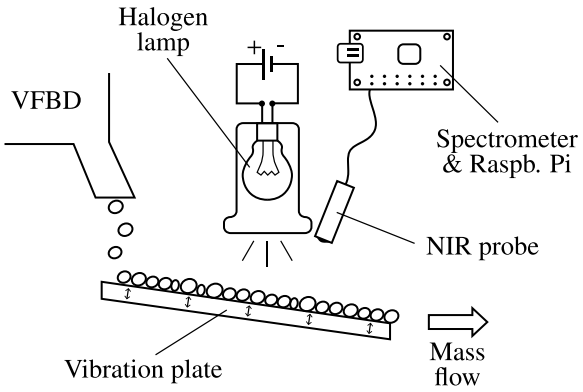

Fig. 4. NIR Sensor setup for residual moisture content inference.

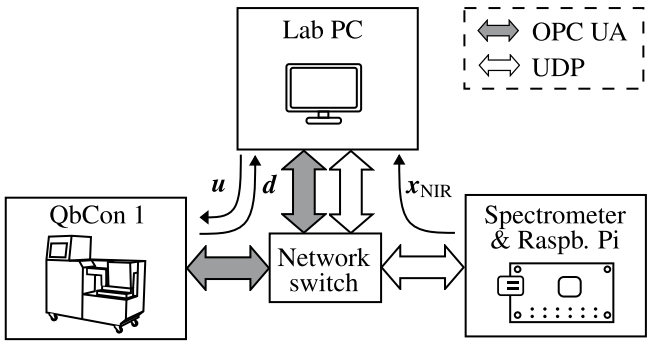

Fig. 5. Communication between the lab PC, the spectrometer, and the QbCon® 1 via Ethernet.

recorded to fit a suitable model. As a reference for calibration, several LOD measurements were taken at various process settings. This ensures that in the subsequent model development, effects related to particle size distribution or mass flow can be adequately separated from the effects of granule moisture.

The calibration dataset, which is freely available in [45], consists of LOD measurements $y_{\mathrm{LOD},k}$ and the respective recorded NIR spectra. Samples of approximately 3 g were taken directly from the product stream immediately downstream of the probe. All spectra recorded within 6 s of the sampling time interval were averaged and added to the training dataset. Several preprocessing steps are applied to the measured spectra. Each spectrum is normalized to the interval $[0, 1]$. A Savitzky–Golay filter of order 1 and window size 3 is applied. Finally, the first derivative of the spectrum is taken, which is obtained from the Savitzky–Golay filter. The variable $\boldsymbol{x}_{\mathrm{NIR},k} \in \mathbb{R}^{N_{\mathrm{NIR}}}$ is the preprocessed spectrum data vector corresponding to the LOD measurement $y_{\mathrm{LOD},k}$. The dataset is hence given by:

$$\boldsymbol{Y}_{\mathrm{LOD}} = \begin{bmatrix} y_{\mathrm{LOD},1} \\ y_{\mathrm{LOD},2} \\ \vdots \\ y_{\mathrm{LOD},m_{\mathrm{NIR}}} \end{bmatrix}, \quad \boldsymbol{X}_{\mathrm{NIR}} = \begin{bmatrix} \boldsymbol{x}_{\mathrm{NIR},1}^{\mathrm{T}} \\ \boldsymbol{x}_{\mathrm{NIR},2}^{\mathrm{T}} \\ \vdots \\ \boldsymbol{x}_{\mathrm{NIR},m_{\mathrm{NIR}}}^{\mathrm{T}} \end{bmatrix}. \tag{30}$$

The dataset consists of $m_{\mathrm{NIR}} = 84$ data points.

PLS regression [46] is often used to relate $\boldsymbol{X}_{\mathrm{NIR}}$ and $\boldsymbol{Y}_{\mathrm{LOD}}$ because it can handle the collinearity of the predictors $\boldsymbol{X}_{\mathrm{NIR}}$. This is achieved by projecting $\boldsymbol{X}_{\mathrm{NIR}}$ into a lower-dimensional subspace of dimension $n_{\mathrm{PLS}} < N_{\mathrm{NIR}}$ similar to principle component analysis (PCA). In contrast to PCA, the subspace is not chosen to cover the largest amount of variance of the predictors $\boldsymbol{X}_{\mathrm{NIR}}$, but instead to maximize the correlation with the observed variables $\boldsymbol{Y}_{\mathrm{LOD}}$. This is beneficial since components with low variance might be more important in predicting the output. PLS regression results in a linear model for the estimated moisture content y_{NIR}:

$$y_{\mathrm{NIR}} = a_{\mathrm{PLS}} + \boldsymbol{b}_{\mathrm{PLS}}{}^{\mathrm{T}} \boldsymbol{x}_{\mathrm{NIR}}. \tag{31}$$

The only hyperparameter of the PLS algorithm is the number of components n_{PLS}. This parameter was chosen such that the leave-one-out cross-validation error on the calibration dataset was minimized. We used the mean square error (MSE) as a measure of fit and performed an exhaustive search of all possible numbers of components. On the given dataset, $n_{\mathrm{PLS}} = 2$ was optimal. Considering the number of granule CQAs that can influence the NIR reflectance — namely particle size and moisture content — this number of latent structures is to be expected.

5. Experimental evaluation

5.1. Experimental setup

This paper presents experimental validation of the developed controller on the QbCon® 1 lab-scale wet granulation line. The QbCon® 1 implements the three unit operations dosing, twin-screw wet granulation, and drying, which it can run fully continuously with a solid mass throughput of 0.5–2.5 kg h^{-1}. The process is retrofitted with additional PAT in the form of a NIR sensor as described in chapter 4.

Granulation of a pre-mixed powder blend is performed on the twin-screw granulator integrated in the QbCon® 1 system. The pre-mixed powder blend consists of alpha-lactose monohydrate (GranuLac® 200, Meggle, Wasserburg am Inn, Germany), microcrystalline cellulose (Vivapur® 101, JRS Pharma, Rosenberg, Germany), and polyvinylpyrrolidone K 90 (Plasdone™ k-90, Ashland Industries Deutschland, Düsseldorf, Germany). It is combined with demineralized water as a granulation liquid. We configured the twin-screw granulator with two kneading zones and a constant screw speed of 250 min^{-1}. The solid mass flow rate remains constant at $\dot{m}_{\mathrm{s,in}} = 1.5\,\mathrm{kg\,h^{-1}}$. After granulation, the granules enter the VFBD, which is controlled by the developed NMPC.

The control algorithms run on a lab PC (Intel® Core™ i7-1260P, 32 GB DDR4 RAM) in MATLAB/Simulink. The lab PC communicates with the QbCon® 1 and the NIR probe via an Ethernet connection and a network switch. The connection to the QbCon® 1 is realized through OPC UA. The QbCon® 1 provides an OPC UA server for this purpose. The lab PC writes the control variables $\boldsymbol{u}$ and reads the disturbances $\boldsymbol{d}$, which are measured by the internal sensors of the QbCon® 1. Read and write requests are sent by the lab PC. If the QbCon® 1 receives no new control input, the last received value is held constant.

The Raspberry Pi receives sensor data from the NIR spectrometer and sends the most recent spectrum $\boldsymbol{x}_{\mathrm{NIR}}$ to the lab PC via UDP. The lab PC evaluates the PLS model to infer the residual moisture content. MATLAB's Industrial Communication Toolbox is used for sending and receiving the signals on the lab PC. Fig. 5 illustrates the communication between the devices.

5.2. Experimental procedure

Before evaluating the NMPC, the reference and economic target selectors are compared in steady state conditions. For this, four different operating points are tested on each target selector: $y_{\mathrm{ref}} \in \{1\,\%, 3\,\%, 5\,\%, 10\,\%\}$. After steady-state conditions are reached, the power consumption is measured using the power meter FLDS100-DR (B+G E-Tech GmbH, Lauchhammer, Germany). The power consumption is measured ten times over a duration of 90 s.

Two experiments are performed once to evaluate the NMPC with the economic target selector in terms of reference tracking and disturbance rejection, respectively. In the first experiment, the reference for the residual moisture content varies between 3 %–5 %–1 %–10 % to test different operating points as well as the transient control response. In the second experiment, the reference remains constant at a value of 3 %. In this case, the inlet moisture content is varied between 25 %–22 %–28 %–25 %. The inlet moisture content represents a measured disturbance to the control system. In practice, an operator or a separate

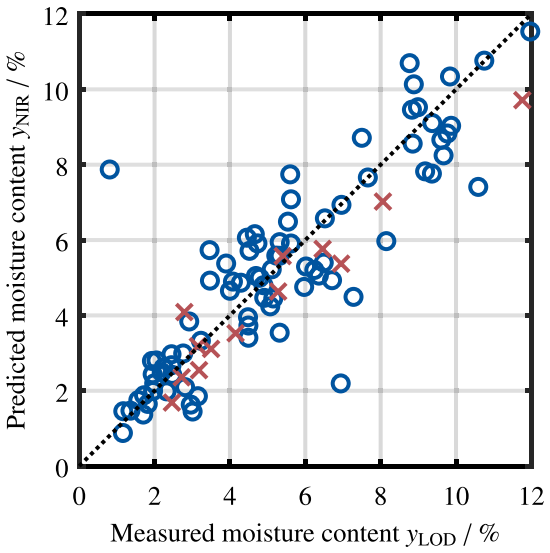

Fig. 6. PLS model prediction compared to LOD measurement for the calibration dataset (circles) and during closed-loop control (crosses).

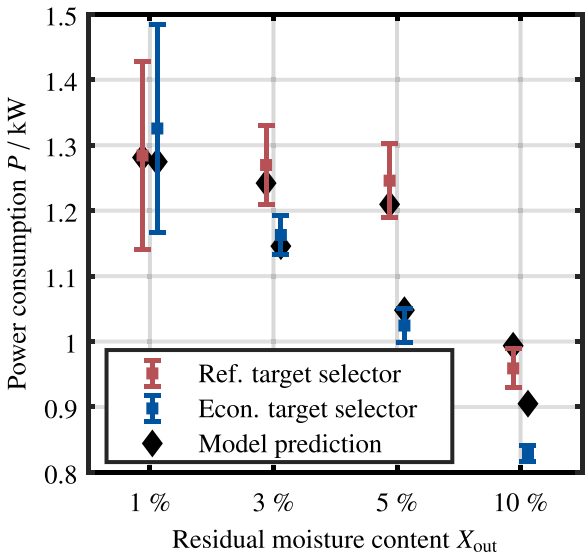

Fig. 7. Comparison of the power consumption using the reference target selector and the economic target selector. The measured power (mean ± standard deviation) is compared with the model (27).

controller might adjust the inlet moisture content to improve the twin-screw granulation performance.

During all experiments, the lab PC logs the measurements of the NIR sensor and of the QbCon® 1. Additionally, at-line LOD measurements are taken with a MA100 (Sartorius, Göttingen, Germany) LOD scale. In contrast to the NIR measurement, the LOD measurement cannot be performed continuously in the product stream. Instead, samples are manually extracted and measured. A new sample is taken every time the measurement of the previous sample is completed.

5.3. Data analysis

Control performance is evaluated based on steady-state errors and transient control performance measures. We consider the steady-state deviations from the reference of both NIR and LOD measurements. The transient behavior is evaluated based on rise time, settling time, and overshoot. For the settling time, we define a ±5 % tolerance around the steady state value. For the rise times, we use a ±10 % tolerance.

6. Results

The results of the PLS regression are shown in Fig. 6. The circles present the leave-one-out prediction of the PLS model for the calibration dataset $\boldsymbol{Y}_{\mathrm{LOD}}$. The leave-one-out cross-validation error in terms of the root mean square error (RMSE) is 1.56 % moisture content. The crosses show a comparison between the LOD measurements taken during the two experiments and the respective PLS predictions based on the NIR measurements. The RMSE between NIR and LOD measurements is 0.96 % moisture content.

The comparison of the reference and economic target selector is illustrated in Table 2 and Fig. 7. Table 2 shows the stationary process parameters as calculated by the two target selectors. The economic target selector chooses, on average, lower values for the air temperature T_{air} and the vibration acceleration a_{vib}. A comparison of power consumption is given by Fig. 7. On average over all measurements, the power consumption with the economic target selector is 104 W lower than with the reference target selector. This corresponds to a reduction of 8.8 % of the total power consumption or a reduction of 26.3 % of the power associated with heating the drying air. Fig. 7 also provides estimates of the power consumption given by (27) with a fitted constant power consumption $P_{\mathrm{const}} = 792$ W. The RMSE between the measurement and the model prediction is 89 W.

Table 2
Stationary process parameters determined by the economic target selector compared to the reference target selector.

	y_{ref} (%)	$\dot{Q}_{\mathrm{air}}$ ($\mathrm{Nm^3h^{-1}}$)	T_{air} (°C)	a_{vib} ($\mathrm{ms^{-2}}$)
Reference target selector	1	30.0	65.2	6.0
	3	24.8	70.3	7.2
	5	23.2	69.9	7.7
	10	13.4	61.7	8.1
Economic target selector	1	30.0	64.6	6.0
	3	25.6	58.3	6.5
	5	25.7	47.6	6.5
	10	14.7	41.3	6.0

Fig. 8 shows the distribution of execution times of the EKF, NMPC, and target selector on the lab PC. The median execution times are 8 ms, 69 ms, and 20 ms, respectively. The median total execution time of all three components is 99 ms, which is well below the sample time $T_{\mathrm{s}} = 1000$ ms. However, there are outliers with much larger execution times. The largest observed total execution time was 1171 ms and the second largest was 518 ms. Thus, one time the controller was not able to be executed within one sample period. In this case, the QbCon® 1 retains the last valid control inputs until a new control input is sent by the lab PC.

Fig. 9 displays the closed-loop control results for the reference tracking experiment. Except for the third set-point, the controller can achieve the desired residual moisture content without a persisting offset in the filtered NIR measurement. During the third set-point of 1 % residual moisture content, only a residual moisture content of 1.9 % was reached. During this time, the outlet granule temperature as predicted by the model approached the allowed maximum of 45 °C. The settling time for the transients during set-point changes cannot meaningfully be calculated due to the strong oscillations of the NIR measurement. The rise times were 203 s, 146 s, and 716 s, respectively. To the last reference change from 1 % to 10 % residual moisture content, the controller reacts with oscillations in the control variables before settling to the steady-state values. The LOD measurement shows some deviation from the filtered NIR measurement. The RMSE was 0.72 % moisture content. In the time frames 41 min $< t <$ 44 min and 49.5 min $< t <$ 50.5 min the controller was not running due to a software error.

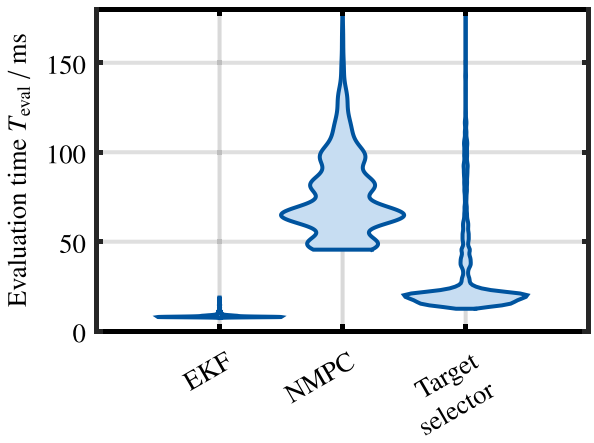

Fig. 8. Distribution of evaluation times of the EKF, NMPC, and target selector.

The results of the disturbance rejection experiment, i.e., the controller's reaction to a change in the inlet moisture content, are displayed in Fig. 10. The variation in the inlet moisture content causes a deviation from the reference in the controlled output. The maximum deviation in the filtered NIR measurement is 2 %.

7. Discussion

Fig. 7 shows that the economic target selector is capable of reducing the power consumption of the process. The reduction in power consumption comes from the reduction of the vibration acceleration compared to the reference target selector. This results in a long drying time and thus reduces the energy consumed by the process. Note that the reduction in vibration does not decrease the process's throughput because, in steady state, the inlet mass flow equals the outlet mass flow. Only the hold-up mass m_{Hup} increases. A disadvantage of the economic target selector is that the vibration acceleration cannot be further reduced in the event of a disturbance. This might negatively influence the dynamic control performance.

The reduction in the total power consumption achieved by the economic target selector is 8.8 %. However, it should be noted that the total energy consumption includes other power consumptions, e.g., from the granulator or internal electronics, which cannot be influenced by the controller.

A comparison between the online NIR measurements and the offline LOD measurements in Figs. 9 and 10 reveals that the NIR measurement can accurately predict the offline measurement. The offline LOD measurement is likely more accurate and can be seen as the ground truth. The raw NIR measurement exhibits substantial measurement noise, as seen from Figs. 9 and 10. For this, there are two likely explanations. The NIR probe measures the NIR spectrum locally on the material stream, i.e., only a small number of particles are measured at a given time. Since the moisture content is not the same in all particles, the measurement has a strong stochastic element. This is amplified by the fact that other stochastically distributed particle properties, such as particle size, may also affect the measured NIR spectrum. The LOD measurement, on the other hand, measures a sample containing a much larger number of particles. This gives an averaged measurement for the particle moisture content.

The second likely contributor to the measurement noise is that the moisture content is inferred through the model (31). Small measurement errors are amplified when propagated through (31) if the model tends towards over-fitting. A higher degree of regularization for the PLS model could be achieved by lowering the number of components n_{PLS}, although this might come at the cost of lower overall prediction performance. Another approach to reduce the model noise sensitivity is the use of model ensembles as described in [28, ch. 5]. Due to the substantial measurement noise, the following discussion will focus on the estimation of the residual moisture content given by the Kalman filter to analyze control performance. It is apparent from Figs. 9 and 10 that the Kalman filter effectively suppresses the measurement noise of the raw NIR measurement. Thus, the effect of measurement noise on control performance is minimized by using physical information from the drying model.

The NMPC successfully achieved offset-free control of the residual moisture content for the set-points 3 %, 5 %, and 10 %. The joint Kalman filter, which estimates the model parameter p, enabled this offset-free control. More precisely, the joint Kalman filter finds a suitable parameter $\hat{p}$ that causes the model prediction to coincide with the measurement. Because the NMPC uses the same model with the same parameter, it can predict the output exactly. This approach attributes the entire model mismatch to the parameter p. Therefore, the estimated value $\hat{p}$ might not exactly equal the physical value of this parameter. Evidently, the entry in the covariance matrix $\boldsymbol{Q}$ corresponding to the value p must be carefully tuned for good noise rejection and convergence speed of the EKF.

The inability of the controller to reach the reference of 1 % residual moisture content is likely due to the granule temperature constraint. As seen from Fig. 9 for a reference of 1 %, the controller operates with the smallest allowed vibration and the largest allowed airflow. Hence, the only way to further decrease the residual moisture content would be to increase the air temperature. This is not possible because it would increase the granule temperature above the specified $T_{\text{max}} = 45\,°\text{C}$. In the presented case, the value for T_{max} was chosen purposefully low to demonstrate the operation of the controller with an active temperature constraint. In practice, this value would be selected based on the processed material. This could be done either from knowledge about the thermal and chemical stability of the API or through experimentation.

The last reference of 10 % residual moisture content is higher than what is sensible in the normal operation of the process. It is chosen only for testing the controller. During the last step change from 1 % to 10 % residual moisture content, the controller strongly increases the vibration acceleration a_{vib}. This way, the residence time is reduced such that a fast transient response can be accomplished. However, after reducing the vibration again, the instationary material flow causes an insufficient amount of material below the NIR probe. This leads to large measurement errors, which can be seen in Fig. 9 around $t = 73\,\text{min}$. Subsequently, the control variables oscillate before eventually settling at the new steady-state values. To improve the results, the tuning of the NMPC should be adjusted, such that the cost associated with changing the vibration acceleration increases.

The rise times of the controller are around 3 min. This value is satisfactory for the considered application. In an industrial application of the controller, the individual operating points will typically be held for a much longer duration than shown in Fig. 9. Therefore, the time needed by the controller to reach steady-state is comparatively small.

Fig. 10 shows the controller's reaction to a change in inlet moisture content. The reaction of the controller is best observed in the large change of inlet moisture content from 22 % to 28 %. Since the inlet moisture content is a measured disturbance, the controller can immediately increase the drying air temperature to counteract the disturbance. Due to model mismatch, the measured residual moisture content falls below the reference. This causes the drying air temperature to briefly decrease before settling at 70 °C. Due to the target selection, the controller only uses the air temperature to counteract disturbances. This is advantageous for energy conservation, but it comes at the cost of control performance because changing the air temperature is slower than changing the vibration and the airflow. If necessary, the controller can be tuned to reduce the cost of deviating from the economic target.

The described experiments already cover a wide range of operating scenarios. Especially, the variation of inlet moisture content is a substantial process disturbance. However, in this contribution, we limited

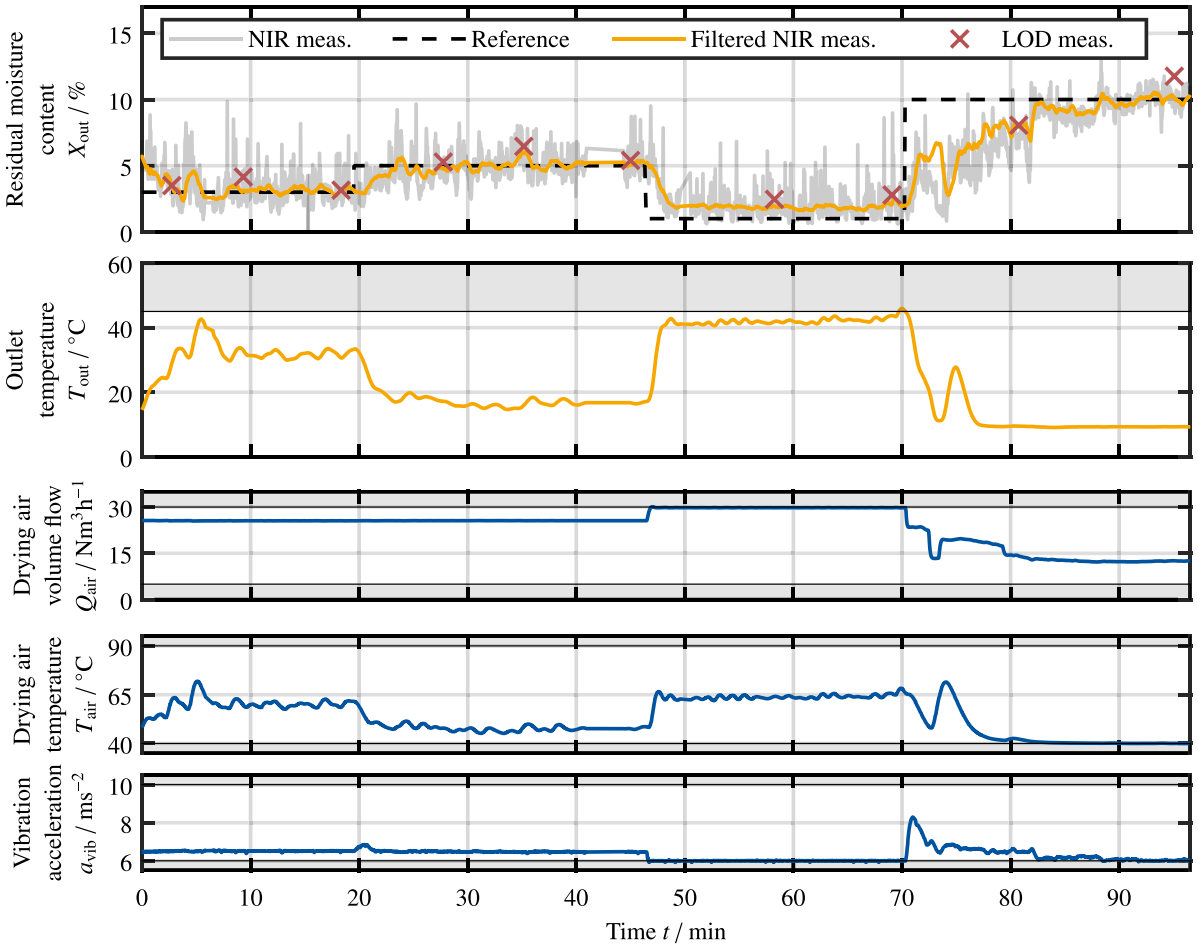

Fig. 9. Reference tracking performance of the developed controller. The upper plot shows the raw NIR measurement (gray), the EKF estimation of the residual moisture content (orange), and the LOD measurements (bordeaux). The outlet temperature was estimated using model (1b). The three control variables, drying air volume flow, drying air temperature, and vibration acceleration, are given by the three lower plots. Bounds of the control variables and the granule temperature as given by Table 1 are marked by the shaded areas.

the scope to a single unit operation. Thus, in future work, it should be investigated how the controlled process interacts in combination with other unit operations and for other formulations.

The presented results show the effectiveness of the proposed NMPC to control the residual moisture content. In industrial practice, the described drying process is so far not actively controlled but rather operated with constant process parameters. The presented combination of inline NIR moisture measurements and MPC allows the automatic adaptation of the process parameters as a consequence of disturbances, e.g., resulting from upstream processes. Thus, the proposed control scheme is capable of improving product quality in solid oral dosage form manufacturing.

Previously proposed controllers for horizontal fluidized bed drying are PID control [24], state feedback control [23], and linear MPC [25]. As pointed out by [25], the continuous fluidized bed drying process benefits from the feedforward action of MPC due to its long residence time. Compared to linear MPC approaches, our NMPC is computationally more expensive. However, the dynamics of the process are slow and the sample time is large with $T_s = 1\,\mathrm{s}$. As seen by the analysis above, this makes the NMPC computationally feasible and thus applicable in an industrial environment.

Since the previously described controllers were not experimentally verified, it is not possible to quantitatively compare control performance with the NMPC. However, performance improvements can be expected due to substantial nonlinearities in the drying dynamics. These nonlinearities result from the two distinct drying zones present in the process [26]. The NMPC formulation can directly consider these nonlinearities, making the underlying model valid in a much larger operating range. Another major advantage of utilizing the physical nonlinear drying model is that the presented approach aligns well with the QbD concept [18]. The direct use of mathematical system knowledge for control likely aids acceptance of the control system by regulators. Furthermore, the EKF enables process monitoring and supervision of the model accuracy. Finally, the physical model structure enhances scalability to industrial-scale dryers. This is a result of the quite general modeling assumptions and the ability to adapt the scale-dependent number of transfer units online.

8. Conclusion

QbC is an important part of the effort to modernize the pharmaceutical industry. Although some research has been done on this topic, case studies with experimentally verified controllers are still very rare. This paper investigated the use of advanced control techniques for the control of horizontal fluidized bed drying for continuous pharmaceutical manufacturing. The investigated control scheme can control the residual moisture content. By additionally minimizing the energy consumption of the drying process, a reduction of 8.8 % in the total energy consumption was achieved compared to a reference implementation. An online estimation of a physical drying parameter makes the control approach adaptable to different formulations and facilitates scale-up. The controller was tested in a lab-scale production line, showing its potential for use in a manufacturing environment.

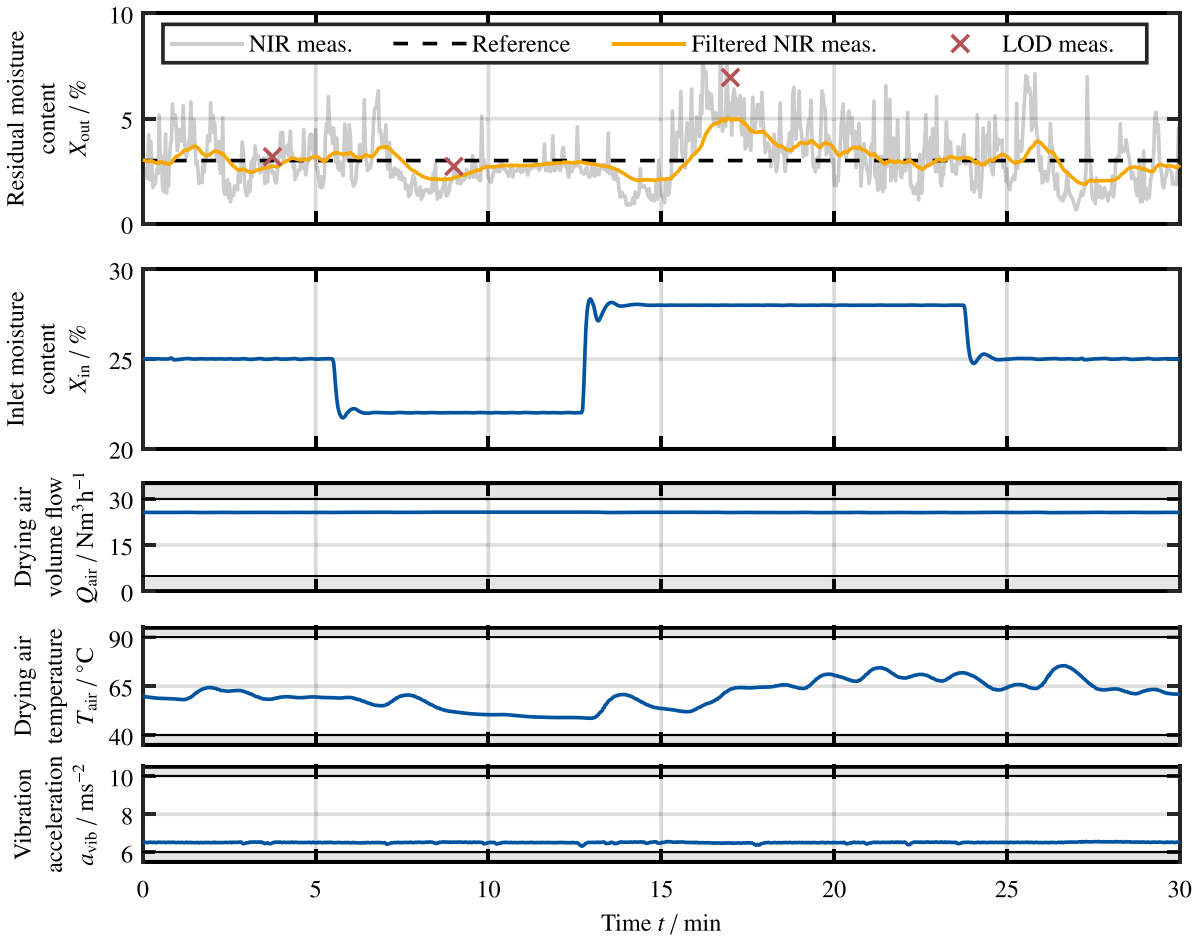

Fig. 10. Disturbance rejection performance of the developed controller for step changes of the inlet moisture content. The upper plot shows the raw NIR measurement (gray), the EKF estimation of the residual moisture content (orange), and the LOD measurements (bordeaux). The three control variables, drying air volume flow, drying air temperature, and vibration acceleration, are given by the three lower plots. Bounds of the control variables and the granule temperature as given by Table 1 are marked by the shaded areas.

QbC relies on advanced PAT to continuously measure the controlled variable. This contribution shows that the control performance depends heavily on the quality of the CQA measurement. The further advancement and adoption of PAT will make QbC more and more viable for many unit operations in drug manufacturing.

In future work, we aim to extend the scope of this work from a single unit operation to the entire tablet manufacturing line. For example, the process parameters of the twin-screw wet granulator were not addressed in this contribution, but can be used to control the particle size distribution, which also has a large impact on final tablet quality. Finally, the effect of intermediate quality attributes on final tablet quality should be investigated. This information can then be used to define set points for intermediate quality attributes of upstream unit operation controllers.

CRediT authorship contribution statement

Stefan R. Tölle: Writing – original draft, Software, Methodology, Investigation, Conceptualization. **Stefan Klinken-Uth:** Writing – review & editing, Software, Investigation, Conceptualization. **Ahmed Elkhashap:** Writing – review & editing, Software, Methodology, Conceptualization. **Alana Delvos:** Writing – review & editing, Investigation. **Heike Vallery:** Writing – review & editing, Project administration. **Jörg Breitkreutz:** Supervision, Project administration. **Sebastian Stemmler:** Writing – review & editing, Supervision, Project administration.

Declaration of competing interest

The authors declare the following financial interests/personal relationships which may be considered as potential competing interests: Institut of Pharmaceutics and Biopharmaceutics reports equipment, drugs, or supplies was provided by LB Bohle Machines and Processes GmbH. Institut of Pharmaceutics and Biopharmaceutics reports equipment, drugs, or supplies was provided by JRS PHARMA GmbH & Co. KG. Institut of Pharmaceutics and Biopharmaceutics reports equipment, drugs, or supplies was provided by MEGGLE GmbH & Co. KG. Institut of Pharmaceutics and Biopharmaceutics reports equipment, drugs, or supplies was provided by Ashland Industries Deutschland GmbH. If there are other authors, they declare that they have no known competing financial interests or personal relationships that could have appeared to influence the work reported in this paper.

Acknowledgments

The authors appreciate the financial support of the German Research Foundation (DFG) received within the research program SPP 2364 “Autonomous processes in particle technology” for the project “Model-based quality control in continuous manufacturing of pharmaceutical granules (QC4CM)” (Nr. 504702251). We would like to acknowledge LB Bohle for their support and for granting access to the QbCon® 1. The authors would also like to thank JRS Pharma, Meggle, and Ashland Industries Deutschland for providing Vivapur® 101, GranuLac® 200, and Plasdone™ k-90.

Data availability

The measurement data and developed controller software required to reproduce the above findings are freely available in the accompanying data publication [45].

References

[1] American Society of Health-System Pharmacists, National drug shortages: January 2001 to september 2024, 2024, https://www.ashp.org/drug-shortages/shortage-resources/drug-shortages-statistics.

[2] ISPE, Drug shortages. A report from the pew charitable trusts and the international society for pharmaceutical engineering, 2017, https://www.pewtrusts.org/en/research-and-analysis/reports/2017/01/drug-shortages.

[3] J. Markarian, Modernizing pharma manufacturing, Pharm. Technol. 42 (4) (2018) 20–25.

[4] I.P. Gabbott, F. Al Husban, G.K. Reynolds, The combined effect of wet granulation process parameters and dried granule moisture content on tablet quality attributes, Eur. J. Pharmaceut. Biopharmaceut. 106 (2016) 7078, http://dx.doi.org/10.1016/j.ejpb.2016.03.022.

[5] S. Sacher, J.G. Khinast, An overview of pharmaceutical manufacturing for solid dosage forms, in: M.G. Ierapetritou, R. Ramachandran (Eds.), Process Simulation and Data Modeling in Solid Oral Drug Development and Manufacture, in: Springer Protocols, Humana Press, New York, 2016, pp. 311–383.

[6] ICH, Q1A (R2): Stability Testing of New Drug Substances and Products – Scientific Guideline, Tech. Rep., 2003.

[7] FDA, PAT – A Framework for Innovative Pharmaceutical Development, Manufacturing, and Quality Assurance, Tech. Rep., 2004.

[8] J. Claßen, F. Aupert, K.F. Reardon, D. Solle, T. Scheper, Spectroscopic sensors for in-line bioprocess monitoring in research and pharmaceutical industrial application, Anal. Bioanal. Chem. 409 (3) (2017) 651–666, http://dx.doi.org/10.1007/s00216-016-0068-x.

[9] E.J. Kim, J.H. Kim, M.-S. Kim, S.H. Jeong, H. Du Choi, Process analytical technology tools for monitoring pharmaceutical unit operations: A control strategy for continuous process verification, Pharmaceutics 13 (6) (2021) http://dx.doi.org/10.3390/pharmaceutics13060919.

[10] ICH, Q13 Continuous Manufacturing of Drug Substances and Drug Products – Scientific Guideline, Tech. Rep., 2022.

[11] S.L. Lee, T.F. O'Connor, X. Yang, C.N. Cruz, S. Chatterjee, R.D. Madurawe, C.M.V. Moore, L.X. Yu, J. Woodcock, Modernizing pharmaceutical manufacturing: From batch to continuous production, J. Pharm. Innov. 10 (3) (2015) 191–199, http://dx.doi.org/10.1007/s12247-015-9215-8.

[12] C.L. Burcham, A.J. Florence, M.D. Johnson, Continuous manufacturing in pharmaceutical process development and manufacturing, Annu. Rev. Chem. Biomol. Eng. 9 (2018) 253–281, http://dx.doi.org/10.1146/annurev-chembioeng-060817-084355.

[13] L.X. Yu, G. Amidon, M.A. Khan, S.W. Hoag, J. Polli, G.K. Raju, J. Woodcock, Understanding pharmaceutical quality by design, AAPS J. 16 (4) (2014) 771–783, http://dx.doi.org/10.1208/s12248-014-9598-3.

[14] Q. Su, S. Ganesh, M. Moreno, Y. Bommireddy, M. Gonzalez, G.V. Reklaitis, Z.K. Nagy, A perspective on quality-by-control (QbC) in pharmaceutical continuous manufacturing, Comput. Chem. Eng. 125 (2019) 216–231, http://dx.doi.org/10.1016/j.compchemeng.2019.03.001.

[15] M. Jelsch, Y. Roggo, P. Kleinebudde, M. Krumme, Model predictive control in pharmaceutical continuous manufacturing: A review from a user's perspective, Eur. J. Pharmaceut. Biopharmaceut. 159 (2021) 137–142, http://dx.doi.org/10.1016/j.ejpb.2021.01.003.

[16] C. Badman, C.L. Cooney, A. Florence, K. Konstantinov, M. Krumme, S. Mascia, M. Nasr, B.L. Trout, Why we need continuous pharmaceutical manufacturing and how to make it happen, J. Pharm. Sci. 108 (11) (2019) 3521–3523, http://dx.doi.org/10.1016/j.xphs.2019.07.016.

[17] ICH, Q8 (R2) Pharmaceutical Development – Scientific Guideline, Tech. Rep., 2009.

[18] F. Destro, M. Barolo, A review on the modernization of pharmaceutical development and manufacturing – Trends, perspectives, and the role of mathematical modeling, Int. J. Pharm. 620 (2022) 121715, http://dx.doi.org/10.1016/j.ijpharm.2022.121715.

[19] K. Kiricenko, P. Kleinebudde, Drying behavior of a horizontal vibrated fluidized bed dryer for continuous manufacturing, Pharm. Dev. Technol. 28 (5) (2023) 440–451, http://dx.doi.org/10.1080/10837450.2023.2205932.

[20] J.A. Villegas, M. Li, S.R. Duncan, H.G. Wang, W.Q. Yang, Modeling and control of moisture content in a batch fluidized bed dryer using tomographic sensor, in: 2008 American Control Conference, IEEE, 2008, pp. 3350–3355, http://dx.doi.org/10.1109/ACC.2008.4587009.

[21] L. Obregón, L. Quiñones, C. Velázquez, Model predictive control of a fluidized bed dryer with an inline NIR as moisture sensor, Control Eng. Pract. 21 (4) (2013) 509–517, http://dx.doi.org/10.1016/j.conengprac.2012.11.002.

[22] F. Gagnon, A. Desbiens, É. Poulin, P.-P. Lapointe-Garant, J.-S. Simard, Nonlinear model predictive control of a batch fluidized bed dryer for pharmaceutical particles, Control Eng. Pract. 64 (2017) 88–101, http://dx.doi.org/10.1016/j.conengprac.2017.04.009.

[23] N.M. Abdel-Jabbar, R.Y. Jumah, M.Q. Al-Haj Ali, State estimation and state feedback control for continuous fluidized bed dryers, J. Food Eng. 70 (2) (2005) 197–203, http://dx.doi.org/10.1016/j.jfoodeng.2004.09.026.

[24] R. Singh, D. Barrasso, A. Chaudhury, M. Sen, M. Ierapetritou, R. Ramachandran, Closed-loop feedback control of a continuous pharmaceutical tablet manufacturing process via wet granulation, J. Pharm. Innov. 9 (1) (2014) 16–37, http://dx.doi.org/10.1007/s12247-014-9170-9.

[25] F. Gagnon, A. Desbiens, É. Poulin, J. Bouchard, P.-P. Lapointe-Garant, Performance of predictive control for a continuous horizontal fluidized bed dryer, J. Process Control 115 (2022) 123–133, http://dx.doi.org/10.1016/j.jprocont.2022.05.007.

[26] S.R. Tölle, S. Klinken-Uth, A. Elkhashap, A. Delvos, J. Breitkreutz, H. Vallery, S. Stemmler, Combined temperature-moisture gray-box model for horizontal fluidized bed drying of pharmaceutical granules, IFAC-PapersOnLine 59 (10) (2025) 1089–1094, http://dx.doi.org/10.1016/j.ifacol.2025.09.184.

[27] R. Meier, Kontinuierliche Feuchtgranulierung und Wirbelschichttrocknung: Experimentelle Untersuchung eines neuartigen, revolutionären Systems, TechnoPharm 8 (3) (2018) 124132.

[28] A. Elkhashap, Nonlinear Model Predictive Control in Continuous Pharmaceutical Production of Solid Dosage Forms (Ph.D. thesis), RWTH Aachen University, Aachen, 2024.

[29] A. Elkhashap, R. Meier, D. Abel, A grey box distributed parameter model for a continuous vibrated fluidized bed dryer in pharmaceutical manufacturing, in: 2020 European Control Conference, ECC, IEEE, Saint Petersburg, 2020, pp. 1415–1421, http://dx.doi.org/10.23919/ECC51009.2020.9143770.

[30] A. Elkhashap, R. Meier, D. Stenger, D. Abel, Grey-box approach for the prediction of variable residence time distribution in continuous pharmaceutical manufacturing, IFAC-PapersOnLine 53 (2) (2020) 10360–10365, http://dx.doi.org/10.1016/j.ifacol.2020.12.2774.

[31] M. Zeller, U. Busweiler, M8 humidifying and drying of air, in: VDI Heat Atlas, Springer, Berlin, Heidelberg, 2010, pp. 1343–1362, http://dx.doi.org/10.1007/978-3-540-77877-6_101.

[32] A. Elkhashap, D. Abel, Reduction and observer design for a grey-box model in continuous pharmaceutical manufacturing, IFAC-PapersOnLine 55 (26) (2022) 26–32, http://dx.doi.org/10.1016/j.ifacol.2022.10.372.

[33] H. Liu, S.C. Galbraith, B. Ricart, C. Stanton, B. Smith-Goettler, L. Verdi, T. O'Connor, S. Lee, S. Yoon, Optimization of critical quality attributes in continuous twin-screw wet granulation via design space validated with pilot scale experimental data, Int. J. Pharm. 525 (1) (2017) 249–263, http://dx.doi.org/10.1016/j.ijpharm.2017.04.055.

[34] R.K. Mandela, R. Rengaswamy, S. Narasimhan, Nonlinear state estimation of differential algebraic systems, IFAC Proc. Vol. 42 (11) (2009) 792–797, http://dx.doi.org/10.3182/20090712-4-TR-2008.00129.

[35] T. Horváth, D. Fodor, Performance comparison of the general the dual and the joint extended Kalman filter on state estimation of Li-ion battery cells for BMS, in: 2024 IEEE 21st International Power Electronics and Motion Control Conference, PEMC, IEEE, Pilsen, Czech Republic, 2024, pp. 1–6, http://dx.doi.org/10.1109/PEMC61721.2024.10726344.

[36] R. Quirynen, B. Houska, M. Vallerio, D. Telen, F. Logist, J. van Impe, M. Diehl, Symmetric algorithmic differentiation based exact Hessian SQP method and software for economic MPC, in: 53rd IEEE Conference on Decision and Control, IEEE, 2014, pp. 2752–2757, http://dx.doi.org/10.1109/CDC.2014.7039811.

[37] J.A.E. Andersson, J. Gillis, G. Horn, J.B. Rawlings, M. Diehl, CasADi: A software framework for nonlinear optimization and optimal control, Math. Program. Comput. 11 (1) (2019) 1–36, http://dx.doi.org/10.1007/s12532-018-0139-4.

[38] A.C. Hindmarsh, P.N. Brown, K.E. Grant, S.L. Lee, R. Serban, D.E. Shumaker, C.S. Woodward, SUNDIALS: Suite of nonlinear and differential/algebraic equation solvers, ACM Trans. Math. Software 31 (3) (2005) 363–396, http://dx.doi.org/10.1145/1089014.1089020.

[39] D.J. Gardner, D.R. Reynolds, C.S. Woodward, C.J. Balos, Enabling new flexibility in the SUNDIALS suite of nonlinear and differential/algebraic equation solvers, ACM Trans. Math. Software 48 (3) (2022) 1–24, http://dx.doi.org/10.1145/3539801.

[40] A. Wächter, L.T. Biegler, On the implementation of an interior-point filter line-search algorithm for large-scale nonlinear programming, Math. Program. 106 (1) (2006) 25–57, http://dx.doi.org/10.1007/s10107-004-0559-y.

[41] R. Verschueren, G. Frison, D. Kouzoupis, J. Frey, N.V. Duijkeren, A. Zanelli, B. Novoselnik, T. Albin, R. Quirynen, M. Diehl, acados – A modular open-source framework for fast embedded optimal control, Math. Program. Comput. 14 (1) (2022) 147–183, http://dx.doi.org/10.1007/s12532-021-00208-8.

[42] Y. Ozaki, C. Huck, S. Tsuchikawa, S.r. Balling Engelsen, Near-Infrared Spectroscopy: Theory, Spectral Analysis, Instrumentation, and Applications, Springer Nature, Singapore, 2021.

[43] D. Mainali, J. Li, P. Yehl, N. Chetwyn, Development of a comprehensive near infrared spectroscopy calibration model for rapid measurements of moisture content in multiple pharmaceutical products, J. Pharm. Biomed. Anal. 95 (2014) 169–175, http://dx.doi.org/10.1016/j.jpba.2014.03.001.

[44] M. Ghijs, B. Vanbillemont, N. Nicolaï, T. De Beer, I. Nopens, Two-dimensional moisture content and size measurement of pharmaceutical granules after fluid bed drying using near-infrared chemical imaging, Int. J. Pharm. 595 (2021) 120069, http://dx.doi.org/10.1016/j.ijpharm.2020.120069.

[45] S.R. Tölle, S. Klinken-Uth, A. Elkhashap, A. Delvos, H. Vallery, J. Breitkreutz, S. Stemmler, An economic model predictive moisture controller for vibrated fluidized bed drying, 2026, http://dx.doi.org/10.18154/RWTH-2026-00498.

[46] V. Esposito Vinzi, G. Russolillo, Partial least squares algorithms and methods, WIREs Comput. Stat. 5 (1) (2013) 1–19, http://dx.doi.org/10.1002/wics.1239.